Comparative study of small scale and 'large scale' resistance spot welding

B. H. Chang, M. V. Li, and Y. Zhou

An incrementally coupled electrical–thermal–mechanical model is developed to simulate small scale resistance spot welding (SSRSW) using the finite element method. This numerical model is then employed to study the differences between SSRSW and 'large scale' resistance spot welding (LSRSW). The variations in contact area, current distribution, and temperature profile at the workpiece/workpiece interfaces are compared. The computation shows that the difference in electrode force could be the essential reason for other differences between SSRSW and LSRSW. Compared with LSRSW, a much lower electrode force (pressure) applied in SSRSW results in a relatively small contact area and hence a much higher current density, which in turn leads to a greater heating rate and higher temperature at the workpiece/workpiece interface. This small contact area also results in a relatively small nugget diameter in SSRSW, which is only about 30% of the electrode tip diameter. In contrast, the nugget diameter in LSRSW is comparable to the electrode tip diameter. The predicted nugget diameters in both SSRSW and LSRSW of mild steel sheets compare well with experimental results. *STWJ/238*

Dr Chang and Dr Zhou (nzhou@uwaterloo.ca) are in the Department of Mechanical Engineering, University of Waterloo, 200 University Avenue West, Waterloo, Ont., N2L 3G1, Canada. Dr Li is in the Edison Welding Institute, 1250 Arthur E. Adams Drive, Columbus, OH 43221, USA. *Manuscript received 3 July 2000; accepted 3 January 2001.*

INTRODUCTION

In the fabrication of electronic components and devices, it is increasingly necessary to resistance weld very thin metal sheets (mostly less than 0·2–0·5 mm in thickness). This application of resistance spot welding (RSW), generally termed as fine, micro-, or small scale resistance spot welding (SSRSW), has many differences compared with the 'large scale' resistance spot welding (LSRSW) that is mainly used for applications in the automotive and appliance industries.[1–5] However, despite this ever increasing necessity to understand SSRSW, little information has been published. In comparison, extensive research and development work (using both experimental and modelling methods) has been carried out in the area of LSRSW of relatively thick sheet metals (mostly greater than 0·6–0·8 mm in thickness).[5]

Because of the lack of directly relevant information, a frequent approach is to 'scale down' the welding conditions suggested for LSRSW (e.g. from Ref. 5) to select the welding parameters for SSRSW. However, it has recently been pointed out that the difference between SSRSW and LSRSW may be due not only to the difference in the scales of the joints, but also to the fundamental difference in the electrode forces used.[2,4] Owing to the very low electrode force (pressure) used in SSRSW, the maximum diameter to which a nugget can grow in SSRSW is limited (only about 30–40% of electrode tip diameter), whereas in LSRSW the nugget and electrode tip diameters are comparable.[4,5]

In the present work, an incrementally coupled electrical–thermal–mechanical finite element model is developed to simulate the SSRSW process and to perform a comparative study on the differences between SSRSW and LSRSW.

LITERATURE REVIEW

In the past decade, computational modelling has become a powerful tool for achieving an improved understanding of the physics associated with the RSW processes. Earlier computational modelling work utilised primarily finite difference methods. Finite element methods (especially using commercial finite element analysis (FEA) packages such as Ansys[6] and Abaqus[7]) are now more commonly used. Excellent reviews on both finite difference models and finite element models of RSW have been presented by Cho and Cho[8] and by Nied.[9] The present paper will highlight the recent developments with a special reference to the progress in the analysis procedure and the modelling of contact resistance.

Analysis procedure

A representative finite difference model is the two-dimensional model by Cho and Cho.[8] This finite difference model solves the coupled thermoelectric problem to simulate the nugget growth process. The contact diameter at the workpiece/workpiece interface is assumed to be twice the electrode face diameter. The contact resistance is a function of temperature dependent surface hardness.

The advantages of finite difference models lie in their simplicity and moderate demand for computing power. However, finite difference models are, in general, not used to solve mechanical problems. Consequently, the interaction between the mechanical and thermal–electrical processes in RSW cannot be appropriately modelled using finite difference methods.

Nied[9] first used Ansys[6] to simulate the squeeze action and obtained the contact radii at the electrode/workpiece and workpiece/workpiece interfaces. It was found that the contact diameter at the workpiece/workpiece interface is about 25% greater than the electrode tip face diameter. Assuming the contact areas remain constant, Nied then conducted coupled thermoelectric analysis to simulate the nugget growth process. The same analysis procedure was adopted and expanded by Tsai and co-workers.[10,11] Regarding materials, Nied studied the nugget growth in stainless steel. Tsai and co-workers investigated both stainless steels[10] and carbon steels.[11]

The analysis procedure used by Nied[9] and by Tsai and co-workers[10,11] ignored the influence of mechanical processes on the conduction of welding current and on the heat generation process. Syed and Sheppard[12] recognised that the contact areas during the RSW process change

continually owing to the interaction between squeeze pressure and thermal expansion in the heated area. To overcome this limitation, they proposed a fully coupled thermal–electrical–mechanical analysis procedure, which involves a significant amount of back and forth iterations for both the thermoelectric and thermomechanical analyses. Such a fully coupled analysis procedure is conceptually rigorous and is a significant step forward in terms of the methodology of RSW modelling. However, this procedure can be very demanding in terms of computing power and its cost may be prohibitive. It is also likely to encounter numerical convergence problems.

Browne *et al.*[13] proposed a more robust procedure, which involves incrementally updating the contact information supplied from the thermal–mechanical analysis using Ansys[6] to the thermal–electric analysis. They used Ansys for their thermal–mechanical analysis and an in house finite difference program to perform the coupled thermal–electrical analysis. Recently such an incrementally coupled thermal–electrical–mechanical analysis procedure has been fully implemented in Ansys by Li *et al.*[14,15] Li *et al.* used the Ansys Parametric Design Language[6] to automate the updating of contact information supplied from the thermal–mechanical analysis to the thermal–electrical analysis at discrete time steps. The whole analysis was performed within Ansys. The concept of this incrementally coupled analysis procedure was also implemented in the Unix operation system using the commercial FEA code Abaqus[7] by Sun *et al.*[16] and Feng *et al.*[17] The implementation involved developing Unix script files as drivers to direct the Abaqus to perform the required analysis tasks.

Contact resistance model

One critical problem in the modelling of RSW is that of quantifying the contact resistance. Browne *et al.*[13] developed a special instrument to measure the dynamic resistance during the welding of aluminium alloys and they artificially adjusted their contact resistance values until a reasonable agreement between the predicted and measured dynamic resistance was reached. Others have used the measured static resistance data and extended them to elevated temperatures based on the dependence of material hardness or yield strength on temperature.[8–11] Apparently both approaches involved a great deal of trial and error, and variability from material to material.

Feng *et al.*[17] recently proposed a phenomenological contact resistance model on the basis of an earlier model proposed by Greenwood.[18] Essentially, they established a relationship to correlate the contact resistance with contact pressure, interface temperature, and electrical resistivity of the materials in contact.

Numerous attempts have been made in the past to measure the contact resistance and to correlate the measured contact resistance with the nugget growth.[19–22] Two major observations can be drawn from these studies: first, all reported measurements have shown marked discrepancies; and second, the measured static resistance values have little correlation with the nugget growth. The widely accepted explanation is that the measured static contact resistance values are attributed mainly to the effects of surface films that are broken down almost instantaneously by the welding current. Studies by Roberts[19] and Thorton *et al.*[22] further identified that film breakdown is caused by the melting of the surface material at dispersed spots at the contact surface. The modelling of contact resistance for the simulation of RSW then depends on the modelling of the contact resistance after film breakdown. Li *et al.*[14] first proposed the description of the contact resistance in a form similar to the Kohlrausch[23] relation. The theory of this contact resistance model can be summarised as follows.

1. Actual contact resistance consists of the film resistance and constriction resistance. Measured static resistance values represent mostly the film effect, which may be orders of magnitude higher than the constriction resistance and sensitive to the surface condition, pressure, and temperature.

2. The welding current breaks down the surface films during the first current cycle and film resistance becomes negligible in comparison with the constriction resistance. Because the film breakdown is associated with the melting and solidification of contact spots, fresh metal–metal contacts are established at the electrode/workpiece and workpiece/workpiece interfaces. Consequently, mathematical characterisation of the constriction resistance is the key to an effective model of the contact resistance, which is highly dynamic in nature in the presence of high magnitude welding currents.

3. Because of the high magnitude of welding current involved in the welding process, the heating rate at the contact interface can be extremely high. However, attempts to heat the contact interface above the solidus temperature of the contact materials will result in instantaneous collapse of the contact spot and increased contact area. Therefore the thermal gradient can be extremely high in the immediate vicinity of the contact interface and a dynamic equilibrium state can be assumed between the heat generation and heat dissipation in the immediate vicinity of the contact interface. It is assumed that the supertemperature[18] at the contact interface remains constant at the solidus temperature of the materials in contact. When the bulk temperature increases above the solidus temperature, contact resistance disappears completely.

4. Fundamentally, the conduction of electricity and heat obey the same form of governing differential equation and these quantities flow through essentially the same pathway. Therefore an isothermal surface may also be a surface of equal potential.[23,24] For an infinitesimal element between two such surfaces, there exists a relation between the thermal resistance $\mathrm{d}W$ and electrical resistance $\mathrm{d}R$

$$\mathrm{d}W = \mathrm{d}R/\rho k \quad . . . . . (1)$$

in which ρ and k are the electrical resistivity and thermal conductivity of the material respectively. Rewriting the Fourier law of heat conduction, the temperature differential between the two isothermal surfaces is then obtained as follows[25]

$$-\mathrm{d}T = q\,\mathrm{d}W = iv\,\mathrm{d}R/\rho k = v\,\mathrm{d}v/\rho k \quad . . . . . (2)$$

where q is the quantity of heat supplied, i is the current and v is the electrical potential with reference to the contact interface.

5. It is known that most pure metals obey the Wiedemann–Franz–Lorentz law

$$\rho k = LT \quad . . . . . (3)$$

where L is the Lorentz constant and T is the temperature in K. It is assumed that the materials involved in the RSW also obey this law. Using the Wiedemann–Franz–Lorentz law, equation (2) can be rearranged as

$$v\,\mathrm{d}v = -LT\,\mathrm{d}T \quad . . . . . (4)$$

Integrating equation (4) over a distance across the contact interface in which the temperature reduces to the bulk temperature, the following relation is obtained

$$V^2 = L(T_S^2 - T_B^2) \quad . . . . . (5)$$

where V is the voltage drop due to constriction resistance on one side of the contact member, T_S is the contact supertemperature required to maintain solid contact, and T_B is the bulk temperature of the interface.

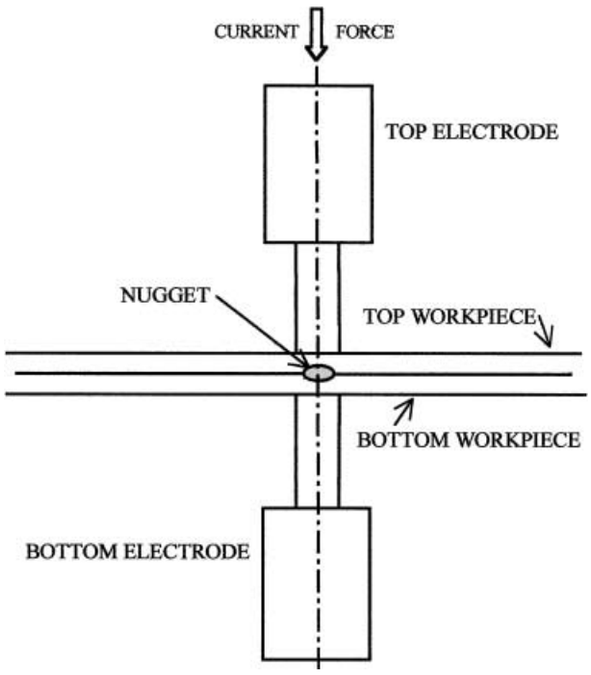

1 Schematic diagram showing apparatus for resistance spot welding

This contact resistance model has reportedly been applied to the analysis of RSW of both uncoated and coated materials. Good agreements were reported between predicted and measured nugget growth data and dynamic resistance.[14,15] Considering that this relation is independent of experimental measurements and therefore avoids the resulting uncertainty, this contact resistance model is employed in the present computations.

Recent studies

Recent work in the modelling of RSW has been focused on the predictions of residual stresses, microstructure, and hardness distribution in the spot welds of high strength steels, as well as the convection effect on the nugget formation.[26–30] The main objective of such research efforts is to correlate the welding process parameters and material chemistry with the mechanical properties of resistance spot welds. The finite element model for RSW of steels can also be used to optimise the welding procedure by accurately controlling the cooling of the weld. This may include introducing online post-weld heat treatment when required.

There is at present no openly published work on the modelling of SSRSW. The present authors have therefore conducted such a study to understand the differences between SSRSW and LSRSW. This work will be especially beneficial for the electronic packaging industry in improving understanding of the SSRSW process and selection of the welding parameters.

FINITE ELEMENT MODEL

The Ansys/MP 5.5[6] FEA code was used in the present work. All computations were carried out on a Pentium 500 personal computer. In the following, details of the geometric model, boundary conditions, and materials properties used in the computation are described.

Geometric model

A typical arrangement for both SSRSW and LSRSW of two metal sheets is shown in Fig. 1. The geometric representation of two identical electrodes and equal thickness workpieces can be simplified to a two-dimensional axisymmetric model, and it is only necessary to construct one-half of the model. Simple cylindrical electrodes with flat tip surfaces are generally used in SSRSW but not so often in LSRSW. For the sake of simplicity and a better comparison between these two processes, cylindrical electrodes with flat tip surfaces are assumed for both SSRSW and LSRSW in the present work.

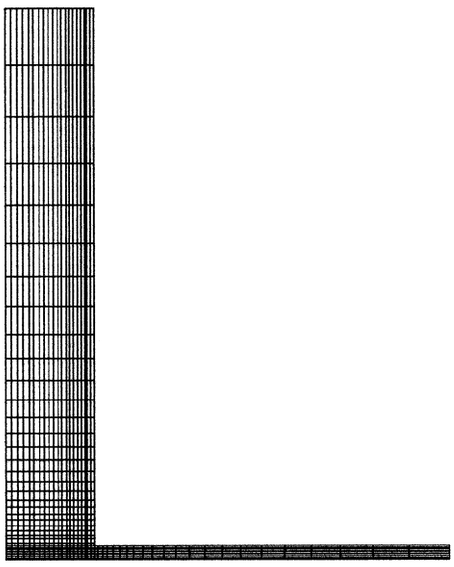

2 One-half of finite element mesh used in numerical analysis

Figure 2 shows the two-dimensional finite element mesh used in the present analysis. Three types of elements in Ansys[6] are used: a thermoelectric solid element for thermal–electrical analysis, an isoparametric solid element for thermal–mechanical analysis, and a node to surface contact element for the coupling at the workpiece/workpiece and electrode/workpiece interfaces. The thermoelectric solid element is used to account for the resistance heating in the workpiece and to calculate the temperature history and distribution. The temperatures obtained are imposed on the isoparametric solid elements as body loads through computer coupling routines. Sequentially, the computation continues to obtain displacements, strains, and stresses, in addition to the actual contact area at the workpiece/workpiece and electrode/workpiece interfaces under mechanical and thermal loads. A thin layer of thermoelectric solid element, having an assumed thickness of 0·01 mm, is used in thermal–electric analysis to simulate the contact resistance.

Refined meshes were assigned to the portion of the workpiece beneath the electrode for SSRSW (Fig. 2). Three mesh sizes ($0{\cdot}16\times0{\cdot}01$, $0{\cdot}08\times0{\cdot}01$, and $0{\cdot}04\times0{\cdot}01$ mm) were used in a convergence study. The results showed that the difference in temperatures and displacements is about 8·0% between $0{\cdot}16\times0{\cdot}01$ and $0{\cdot}08\times0{\cdot}01$ mm meshes, and is only 1·0% between $0{\cdot}08\times0{\cdot}01$ and $0{\cdot}04\times0{\cdot}01$ mm meshes. Therefore, the finest mesh size used in the SSRSW calculation was $0{\cdot}08\times0{\cdot}01$ mm. The mesh construction for SSRSW consists of 1906 nodes and 1708 solid elements, whereas the mesh construction for LSRSW was similar to that used by Li *et al.*[14]

Boundary conditions

The boundary conditions used in the thermal–electrical analysis include the following:

(i) the voltage at the bottom end of the lower electrode is set to zero, and an alternating current (ac) of

frequency 60 Hz is applied at the top end of the upper electrode

(ii) the current is permitted to flow across the electrode/workpiece and workpiece/workpiece interfaces, but not allowed to flow along the lateral surfaces or across the centreline of the electrode

(iii) the outer surfaces are assumed to be adiabatic, which is reasonable since Browne *et al.*[13] have indicated that convective heat transfer to the surrounding air is negligible

(iv) heat transfer across the electrode/workpiece and workpiece/workpiece interfaces is calculated using the node to surface contact elements

(v) in practice, cooling water is used in LSRSW but not in SSRSW: however, for the sake of simplicity and a better comparison between these two processes, no cooling effect is considered in the present work; this assumption has little effect on the temperature characteristics at the workpiece/workpiece interface but may influence the temperature profiles at the electrode/workpiece interfaces in LSRSW

(vi) there is no radial heat flow along the centreline and no vertical heat flow over the contact area of the workpiece/workpiece interface because of symmetry.

The boundary conditions used in the thermal–mechanical analysis include the following:

(i) electrode force is applied as an evenly distributed pressure at the top end of the upper electrode

(ii) axial displacements at the bottom end of the lower electrode are constrained

(iii) radial displacements at the centreline are restricted.

Material properties

Mild steel AISI 1010 and class 2 electrodes are used in the present work. One major reason for the electrical–thermal–mechanical coupling effect is that materials properties depend strongly upon temperature. In the present work, the temperature dependent electrical, thermal, and mechanical property parameters of the electrodes and mild steel are taken from Ref. 11. Details of the workpiece thickness, electrode diameter, and process parameters used in the present work are given in Table 1, which includes two typical sets of welding conditions for SSRSW and LSRSW.[4,14]

The contact resistivities of the contact elements at the electrode/workpiece and workpiece/workpiece interfaces are derived from the Kohlrausch[23] model, which has been described in the previous section. From equation (5), the voltage drop across a contact interface at any bulk temperature T_0 below T_S can be obtained. The temperature dependent contact resistance of the interface can be calculated by dividing the temperature dependent voltage drop by the welding current. Then, the contact resistance values are converted to the equivalent electric resistivity using geometric information from the contact elements at the interface. For a temperature greater than T_S, the electric resistivity of the bulk material, which is again temperature dependent, is used for the contact elements. In the present

Table 1 Welding conditions for small scale (SSRSW) and 'large scale' resistance spot welding (LSRSW)

Parameter	SSRSW	LSRSW
Plate thickness, mm	0·3	0·8
Welding current (ac, rms), kA	0·8	7·0
Electrode force, N	50	2000
Welding time, cycles	10	12
Electrode tip diameter, mm	3·2	6·0

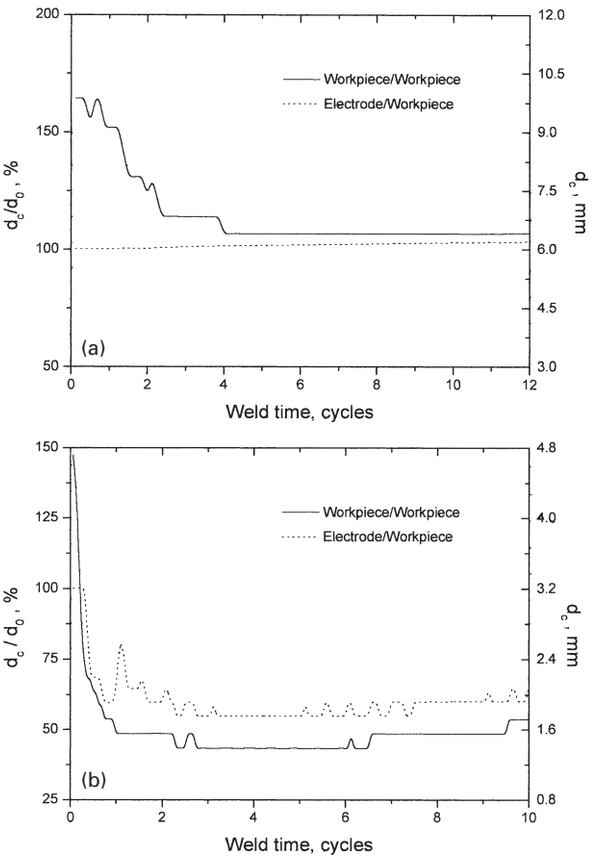

3 Variations of normalised contact diameter d_c at workpiece/workpiece and electrode/workpiece interfaces for *a* 'large scale' (LSRSW) and *b* small scale resistance spot welding (SSRSW): d_0 is electrode tip diameter

computations, T_S at the workpiece/workpiece interface is specified as the solidus of mild steel (1500°C), and that at the electrode/workpiece interface as the melting point of the Cu–Zr electrodes (1084°C). The value of L is not exactly the same for all metals: the value of $2{\cdot}0 \times 10^{-8}$ V^2 K^{-2}, quoted for iron,[31] is used in the present work.

RESULTS AND DISCUSSION

The values of current density and temperature peak when the ac peaks because of the sinusoidal waveform. Therefore, the results in the following sections correspond to the values at the last current peak point for the number of cycles quoted. For example, the results quoted for 2 cycles are actually the values at 1·75 cycles.

Contact area

Figure 3 shows the variations in contact diameter at the workpiece/workpiece and electrode/workpiece interfaces in both SSRSW and LSRSW when the present model is run using the conditions in Table 1. In LSRSW (Fig. 3*a*), the diameter of the contact area at the workpiece/workpiece interface is initially greater than that of the electrode tip face and reduces sharply during welding. This occurs because the resistance heating in the central region of the workpieces leads to a thermal expansion in that region and hence forces the two workpieces to separate at the edge of the mechanically loaded area. It is obvious that the balance between the electrode force and the force resulting from the uneven thermal expansion will determine the amount of reduction in contact area. The contact diameter 'settles' at about the electrode tip diameter at a welding time of

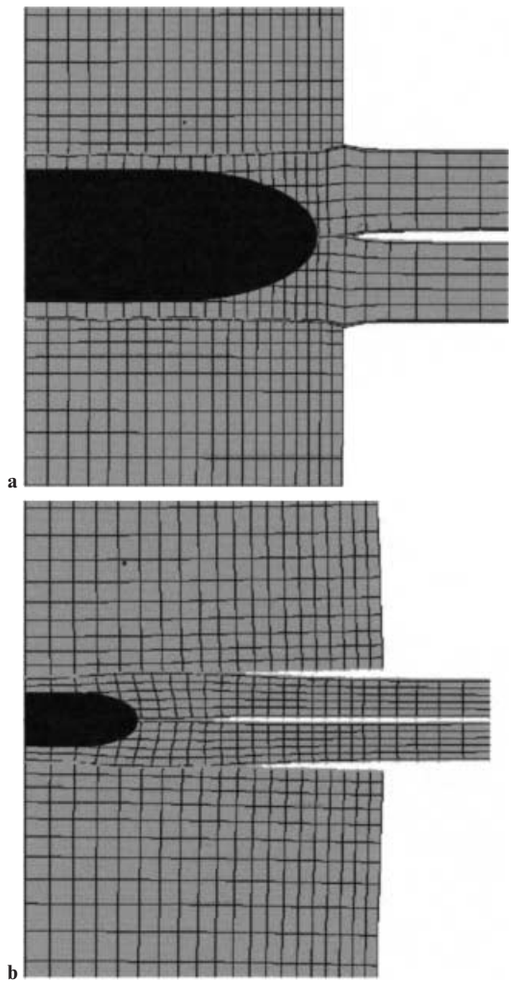

4 Comparison of cross-sections of electrode/workpiece stacks during *a* LSRSW (10 cycles) and *b* SSRSW (4 cycles)

4 cycles and shows little subsequent variation. The reduction in the contact diameter at the workpiece/workpiece interface is significant (from about 170% to 110% of the electrode tip diameter). The variation in contact area at the electrode/workpiece interface is very small compared with that at the workpiece/workpiece interface in LSRSW (Fig. 3*a*).

As shown in Fig. 3*b*, the contact diameter at the workpiece/workpiece interface in SSRSW reduces even more significantly (from about 150% to about 40% of the electrode tip diameter) compared with LSRSW. More importantly, the minimum contact diameter in SSRSW is only about 40% of the electrode tip diameter, whereas that in LSRSW is about the same as the electrode tip diameter. This major difference occurs because the very low electrode force in SSRSW cannot counteract the thermal expansion caused by the electric heating. The change in contact diameter at the electrode/workpiece interface in SSRSW is also different from that in LSRSW. Furthermore, the contact area diameter in SSRSW changes from the initial tip diameter to only about 55% of the initial diameter, whereas the contact area in LSRSW remains similar to the electrode tip area. The contact diameter at the electrode/workpiece interface is slightly greater than that at the workpiece/workpiece interface in SSRSW, whereas those in LSRSW are very close. At longer welding times, the contact areas start to increase because the material is softened at high temperature (Fig. 3*b*).

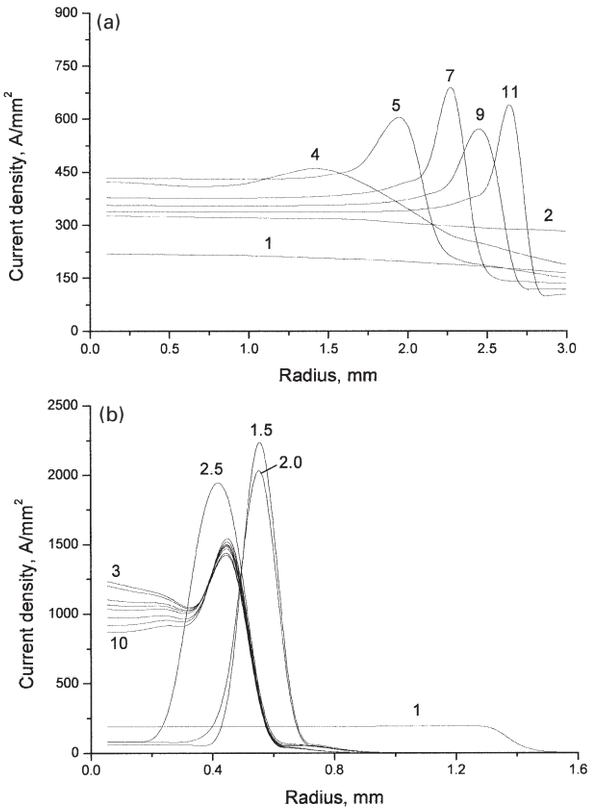

5 Distribution of welding current density at workpiece/workpiece interface at various welding times (shown as numbers of cycles) for *a* LSRSW and *b* SSRSW

Figure 4 shows two graphic presentations of the deformed electrode/workpiece stacks in both LSRSW and SSRSW, which indicate clearly the difference between the contact areas in the two processes. The contact areas in SSRSW are much smaller than the electrode diameter, whereas those in LSRSW are comparable to the electrode diameter. The contact diameter represents the actual area of welding current flow during welding; therefore, the variation of contact diameter will definitely affect the magnitude and distribution of welding current and hence heat generation, and this is discussed in the following subsections.

Welding current density

In RSW, workpieces are welded together through a nugget formed by Joule heating. Mathematically, this can be represented by

$$Q = i^2 Rt \quad \ldots\ldots\ldots\ldots\ldots\ldots \quad (6)$$

where Q is the heat generation, i is the welding current, R is the resistance of the workpiece, and t is the duration of current application (welding time). Therefore, the welding current is the most significant variable affecting nugget formation and growth because the heat generated is proportional to the square of the welding current. To compare the effect of welding current in LSRSW and SSRSW, the variation in current density at the workpiece/workpiece interfaces during welding is plotted in Fig. 5. The nominal current density (i.e. welding current divided by section area of the electrode) is about 140 A mm^{-2} in SSRSW and about 350 A mm^{-2} in LSRSW.

The distribution of the welding current at the workpiece/workpiece interface in LSRSW changes greatly during the welding process (Fig. 5*a*). At the start of welding, the

current density distribution is relatively uniform across the contact area, but the current density is below the nominal value (350 A mm^{-2}) because the contact area is larger than the electrode tip area (Fig. 3*a*). As the welding time increases, the average current density approaches the nominal value because the contact area is reduced to approximately the tip surface area. However, the current is no longer uniformly distributed: the current density is higher in the central region of the contact area than that at the edge. This is because the temperature in the central region is higher and hence the contact resistance is lower, and the current tends to flow into the low resistance area. Once a molten nugget is formed (when the welding time is about 5 cycles in Fig. 5*a*), the current density in the nugget region is much higher than that in the non-melted region because the contact resistance in the molten region disappears. In addition, there is a peak current density at the nugget periphery due to the 'edge effect', in which the current tends to flow into the nugget periphery because of the lower resistance in this area compared with the non-melted regions. The resistance in the central nugget region is also higher because of the higher temperature than that at the nugget periphery. The location of the current density peak moves away from the nugget centre as the nugget grows (Fig. 5*a*). At the same time, the average current density in the nugget region decreases as the nugget grows because the lower resistance region enlarges.

The change in SSRSW is much more complex than that in LSRSW. The current density changes very rapidly from a uniform distribution initially to a highly uneven distribution when the welding time is about 1–3 cycles, and to a distribution similar to that for LSRSW after the 3rd cycle, where the current concentrates in the molten nugget regions. The current density is about 200 A mm^{-2} during the 1st cycle, which is already higher than the nominal current density in SSRSW because of the rapid reduction in contact area (Fig. 3*b*). At welding times of about 1·5 and 2·5 cycles, the current density peaks at about 2000 A mm^{-2} at diameters of 0·6 and 0·4 mm respectively, which is due to the surface melting in these regions (*see* following subsection). Once a molten nugget is formed at the weld centre (at welding times greater than 3 cycles), the current density distributions become similar to those in LSRSW when a molten nugget is formed, except that the current density values are much higher than those in LSRSW. However, the current density peak moves towards the nugget centre when the welding time changes from 1·5 to 2·5 cycles (Fig. 5*b*), which is the opposite behaviour to that observed in LSRSW (Fig. 5*a*). This is due to local melting during the reduction of contact diameter in SSRSW, which will be discussed in the following subsection (Fig. 6*b*). It is also very interesting to note that the significant reduction in contact area increases the current density in SSRSW to a level much higher than that in LSRSW although the nominal current density in SSRSW is much lower. As can be seen below from the analysis of temperature distribution, it is the much higher current density in SSRSW that leads to a more rapid increase in temperature, and hence less welding time is required for a nugget to initiate and grow to its full size compared with LSRSW.

Temperature distribution

Temperature distribution is fundamentally important in RSW since it affects when the molten nugget will initiate and how large the nugget can grow. This in turn influences other properties, such as microstructures in the nugget and heat affected zone, and mechanical behaviour of the welded joints. Therefore, the differences in temperature distributions between LSRSW and SSRSW have been studied in detail.

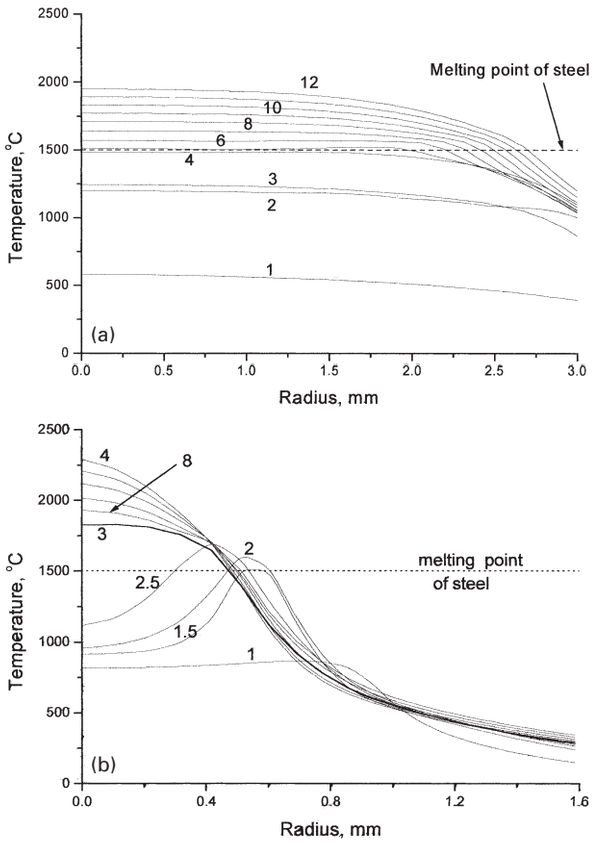

6 Temperature distribution at workpiece/workpiece interface at various welding times (in cycles) for *a* LSRSW and *b* SSRSW

Figure 6*a* shows the temperature distribution at the workpiece/workpiece interface in LSRSW. Temperature increases very rapidly initially and melting occurs when the welding time is about 4 cycles. Once a molten nugget is formed, the temperature increases at a lower rate because the contact resistance is greatly reduced. The nugget grows continually to its maximum value (close to the electrode tip diameter) until about 12 cycles welding time. Further passage of welding current has little effect on the temperature distribution.

Compared with LSRSW, the temperature at the workpiece/workpiece interface in SSRSW initially increases at a much higher rate because of the greatly reduced contact area; moreover, the temperature distribution is also much less uniform, as shown in Fig. 6*b*. It is very interesting to note that at welding times of 1·5 and 2·5 cycles, melting occurs in rings at locations about 0·8 and 1·2 mm in diameter, which is the reason for the current peaks at these locations shown in Fig. 5*b*. This molten region is limited to the interface vicinity and, as the welding time increases, the temperature in the regions decreases below the melting point. If the above prediction is correct, the surface melting regions should be discernible. Figure 7 shows two scanning electron microscopy images of a fractured surface from a SSRSW joint made using a welding time of 1 cycle (other welding conditions are as given in Table 1). The micrographs show a fractured nugget about 0·3 mm in diameter (A in Fig. 7) at the weld centre and three rings (B, C, and a third between B and C). These rings appear to have experienced much higher temperature than the other areas except for the nugget region A, and the temperature at ring B was higher than that at ring C. Judging from the many small fractured areas present (Fig. 7*b*), ring B was at least

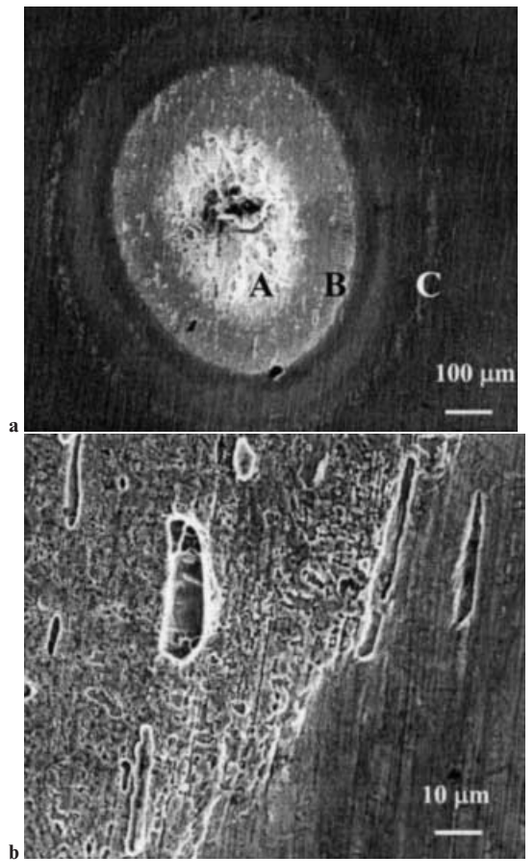

7 Fracture surface of weld produced using SSRSW with welding time of 1 cycle: *b* shows detail of region B in *a* (SEM)

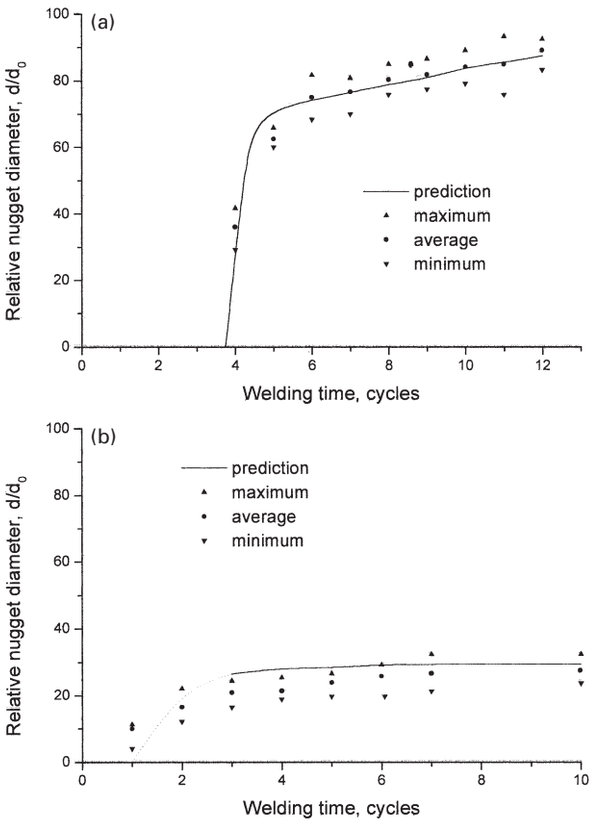

8 Comparison of calculated nugget diameter results with experimental data for *a* LSRSW and *b* SSRSW (experimental data for LSRSW are from Ref. 14)

partially melted. Therefore, the numerical model developed in the present work has fairly effectively predicted the high temperature rings in SSRSW. It can also be seen from Fig. 7 that the melting at ring B is very superficial and hence will make little contribution to the joint strength because of the limited dimensions of the melted regions. The calculation predicts that a molten nugget is formed at the weld centre when the welding time is about 3 cycles (Fig. 6), and this nugget grows little after 4 cycles. The maximum nugget diameter in SSRSW is only about 30% of the electrode tip diameter.

To summarise the above discussions concerning contact diameter, current density distribution, and temperature profiles, it is evident that the difference in electrode force (pressure) applied in LSRSW and SSRSW is the dominant reason for all other differences between these two processes. Compared with LSRSW, a much lower electrode force in SSRSW results in a relatively small contact area and hence a much higher current density leading to a more rapid heating rate, shorter threshold welding time, and higher temperature in the nugget region. The small contact area also results in a relatively small nugget, which is only about 30% of the electrode tip diameter, whereas the nugget diameter in LSRSW is comparable to the electrode tip diameter.

Comparison with experimental results

Comparisons have been made between the predicted nugget diameter and those obtained in experiments. The experimental results for LSRSW are from a previous work.[14] The SSRSW process was performed using the parameters in Table 1; no cooling water was used for SSRSW and methanol was used to clean the steel sheets before welding.

Figure 8 shows the plots of nugget diameter versus welding time for both LSRSW and SSRSW, in which the nugget diameters have been normalised to the respective electrode tip diameters. It can be seen from Fig. 8 that the predicted nugget diameters compare reasonably well to the experimentally measured results. The diameter of the fully developed nugget in LSRSW is comparable to the electrode tip diameter (6 mm), whereas that in SSRSW is only about 30% of the electrode tip diameter (3·2 mm). The threshold welding time in SSRSW is also much shorter than that in LSRSW. All the experimental data are reasonably well predicted by the present model.

However, determination of the threshold welding time for SSRSW is problematic. As indicated in the previous subsection, the melting first occurred at the ring regions when the welding time was about 1–2 cycles; however, these rings contributed little to the joint strength. This is also confirmed in Fig. 8*b*, where the nugget diameters correspond to the calculated diameters of the molten nugget at the weld centres, but not to the maximum diameters of these ring regions. Therefore, the threshold welding time should be defined as that when a molten nugget is formed at the weld centre (at about 3 cycles) although the first melting at the ring regions is after about 1–2 cycles. A broken line is drawn between 1 and 3 cycles in Fig. 8*b* to show that the melting did occur before 3 cycles. Whether the predicted threshold welding time is 1–2 cycles or 3 cycles, the numerical model has underpredicted the threshold welding time for SSRSW since the experimental results indicate that a molten nugget is already formed after a welding time of 1 cycle. This should be linked to the assumption made for the contact resistance model, in which the film resistance is not taken into account. Although this assumption works well for LSRSW, in which the threshold welding time for

nugget initiation is longer than that for surface film breakdown (which occurs at about the 1st cycle[14]), it causes some error in predicting a threshold welding time that is very short in SSRSW.

CONCLUSIONS

1. The difference in electrode forces used in SSRSW and LSRSW is the dominant reason for other differences between SSRSW and LSRSW.

2. Contact diameters at both workpiece/workpiece and electrode/workpiece interfaces are similar to the electrode tip diameter in LSRSW. However, contact diameters at both interfaces in SSRSW are greatly reduced and much smaller than the electrode tip diameter, because the low electrode force cannot counteract the local thermal expansion of the workpieces.

3. In both SSRSW and LSRSW, the current density is higher in the nugget region. The current density in SSRSW is significantly higher than that in LSRSW because of a greatly reduced contact area in SSRSW, although the nominal current density in SSRSW is lower than that in LSRSW.

4. The heating rate and peak temperature are much higher in SSRSW compared with LSRSW because of the much higher current density in SSRSW.

5. The calculated nugget diameter compares well with experimental observations during SSRSW and LSRSW of mild steel. Also, the predicted high temperature rings at the workpiece/workpiece interface in SSRSW were observed in experiments.

ACKNOWLEDGEMENTS

The authors would like to acknowledge financial support from the Natural Sciences and Engineering Research Council (NSERC) in Canada.

REFERENCES

1. Y. ZHOU, C. REICHERT, and K. J. ELY: Proc. Conf. on 'Joining applications in electronics and medical devices' (ICAWT '98), Columbus, OH, September 1998, Edison Welding Institute, 79–90.
2. Y. ZHOU, P. GORMAN, W. TAN, and K. J. ELY: *J. Electron. Mater.*, 2000, **29**, (9), 1090–1099.
3. W. R. BRATSCHUN and J. L. LEICHT: *IEEE Trans. Comp. Hybrids Manuf. Technol.*, 1992, **15**, (6), 931–937.
4. K. J. ELY and Y. ZHOU: *Sci. Technol. Weld. Joining*, 2001, **6**, 63–72.
5. 'Resistance welding manual', 4th edn, Chap. 14; 1989, Philadelphia, PA, Resistance Welder Manufacturers' Association.
6. Ansys, *see* www.ansys.com.
7. ABAQUS, *see* www.hks.com.
8. H. S. CHO and Y. J. CHO: *Weld. J.*, 1989, **68**, (6), 236s–244s.
9. H. A. NIED: *Weld. J.*, 1984, **63**, (4), 123s–132s.
10. C. L. TSAI, O. A. JAMMAL, J. C. PAPRITAN, and D. W. DICKINSON: *Weld. J.*, 1992, **71**, (2), 47s–54s.
11. C. L. TSAI, W. L. DAI, D. W. DICKINSON, and J. C. PAPRITAN: *Weld. J.*, 1991, **70**, (12), 339s–351s.
12. M. SYED and S. D. SHEPPARD: in 'Modeling and control of joining processes', (ed. T. Zacharia), 422–429; 1993, Materials Park, OH, ASM/AWS. 13
13. D. J. BROWNE, H. W. CHANDLER, J. T. EVANS, and J. WEN: *Weld. J.*, 1995, **74**, (10), 339s–344s.
14. M. V. LI, P. DONG, and M. KIMCHI: Proc. 7th Int. Conf. on 'Computer technology in welding', San Francisco, CA, July 1997, NIST, 423–434.
15. M. V. LI, P. DONG, and M. KIMCHI: Proc. 7th Int. Conf. on 'Computer technology in welding', San Francisco, CA, July 1997, NIST, 389–398.
16. X. SUN, P. DONG, and M. KIMCHI: Proc. 7th Int. Conf. on 'Computer technology in welding', San Francisco, CA, July 1997, NIST, 447–457. 14
17. Z. FENG, J. E. GOULD, S. S. BABU, M. L. SANTELLA, and B. W. RIEMER: in 'Trends in welding research: proceedings of the 5th international conference', (ed. J. M. Vitek *et al.*), 599–604; 1998, Materials Park, OH, ASM International.
18. J. A. GREENWOOD: *Br. J. Appl. Phys.*, 1967, **17**, 1621–1632.
19. W. L. ROBERTS: *Weld. J.*, 1951, **30**, (12), 1004–1019.
20. J. G. KAISER, G. J. DUNN, and T. W. EAGAR: *Weld. J.*, 1982, **61**, (2), 167s–174s.
21. M. M. VOLGER and S. D. SHEPPARD: *Weld. J.*, 1993, **72**, (6), 231s–238s.
22. P. H. THORTON, A. R. KRAUSE, and R. G. DAVIES: *Weld. J.*, 1996, **75**, (12), 402s–412s.
23. F. KOHLRAUSCH: *Ann. Phys. (Leipzig)*, 1900, **1**, 312. 15
24. R. HOLM and E. HOLM: 'Electric contacts: theory and application', 4th edn; 1967, New York, Springer-Verlag. 16
25. M. V. LI and M. KIMCHI: submitted to *Sci. Technol. Weld. Joining.* 17
26. M. L. SANTELLA, S. S. BABU, B. W. RIEMER, and Z. FENG: in 'Trends in welding research: proceedings of the 5th international conference', (ed. J. M. Vitek *et al.*), 605–609; 1998, Materials Park, OH, ASM International.
27. M. V. LI, P. DONG, and M. KIMCHI: in 'Trends in welding research: proceedings of the 5th international conference', (ed. J. M. Vitek *et al.*), 155–160; 1998, Materials Park, OH, ASM International.
28. M. V. LI, Z. FENG, and M. KIMCHI: Proc. Conf. 'SEM annual conference on theoretical, experimental and computational mechanics', Cincinnati, OH, June 1999, 850–852.
29. P. S. WEI, S. C. WANG, and M. S. LIN: *J. Heat Transfer*, 1996, **118**, (8), 762–773.
30. J. A. KHAN, L. XU, Y. J. CHAO, and K. BROACH: *Numer. Heat Transfer A*, 2000, **37**, (5), 425–446.
31. H. N. WAGAR: in 'Integrated device and connection technology', (ed. D. Baker *et al.*), 439–499; 1971, Englewood Cliffs, NJ, Prentice-Hall.

AUTHORS QUERIES

Journal: **Science and Technology of Welding and Joining**
Paper: **STWJ/238**

Dear Author
During the preparation of your manuscript for publication, the questions listed below have arisen. Please attend to these matters and return this form with your proof. Many thanks for your assistance

Query Reference	Query	Remarks
1	Author: Is the title for Li OK?	
2	Author: Is 'supplied from' OK? If not, please clarify.	
3	Author: Is 'supplied' OK? If not, please clarify.	
4	Author: Is the definition of 'q' OK?	
5	Author: Is 'contact supertemperature required to maintain solid contact' OK, as reworded?	
6	Author: Is 'between 0.08×0.01 and 0.04×0.01 mm' OK? Original had 0.16×0.01 vs 0.08×0.01 again, as at start of sentence.	
7	Author: Is 'similar to' OK, as not exactly equal?	
8	Author: Is 'other welding conditions are as given in Table 1' OK?	
9	Author: Is 'limited dimensions of the melted regions' OK?	
10	Author: Is 'in SSRSW' OK?	
11	Author: Is 'predicted' OK? If not, please clarify this whole sentence.	
12	Author: Would 'overestimated' be clearer in this context?	
13	Author: In Ref. 12, is the amended page range '422–429' correct?	

14	Author: In Ref. 16, is the author 'X. Sun' OK?	
15	Author: In Ref. 23, is the journal title 'Ann. Phys' OK?	
16	Author: Is it OK that there are no page numbers in Ref. 24, i.e. reference to whole book?	
17	Author: Have Ref. 25 been accepted? Any further details?	